a. Expression of *vgll3* in male and female gonads

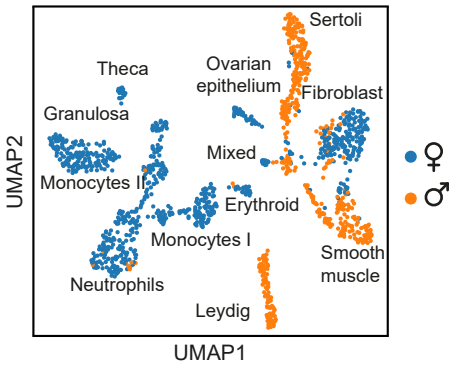

b. Cell type-specific *vgll3* expression

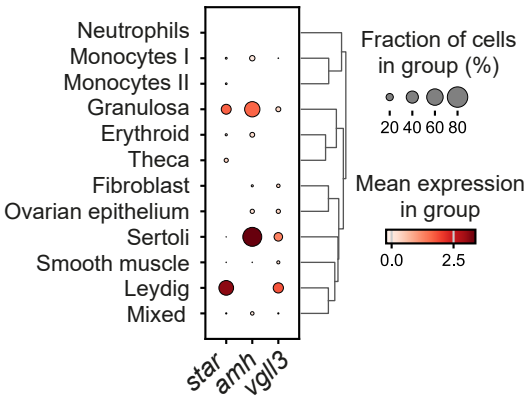

c. smFISH for selected markers in the testis

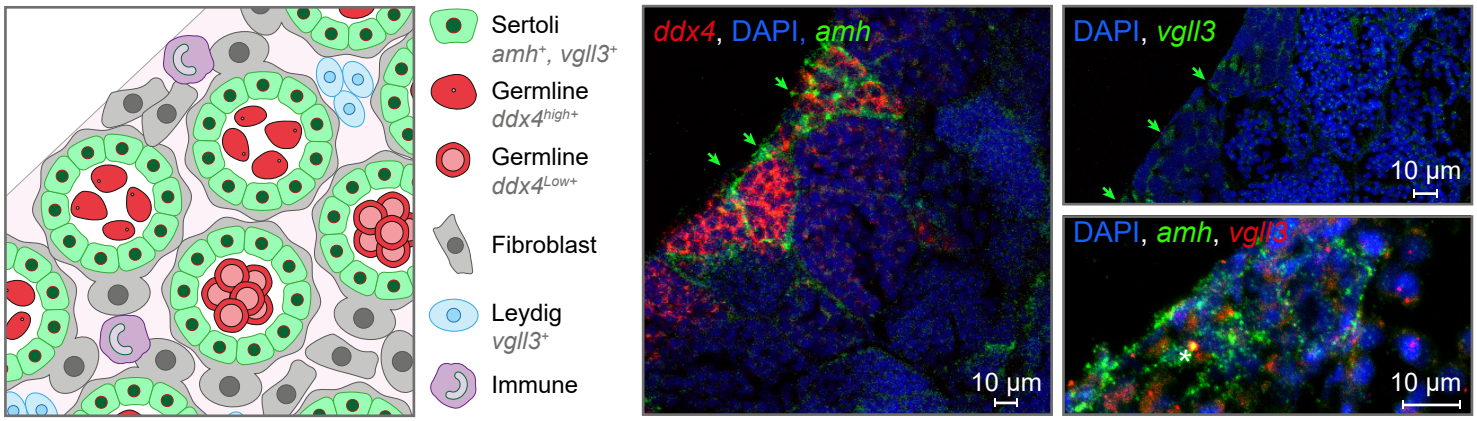

Supplementary Figure 1: *vgll3* expression in gonadal support cells

a) UMAP analysis of single cells from the testes and ovaries of 1-month-old fish (data from[1]), depicting somatic cells, which are clustered and color-coded by sex of origin.

b) Dot plot representing the relative expression of selected cell-type-specific marker genes (according to[1]), including *vgll3*.

c) Left: a model illustrating the spatial distribution of primary gonadal cell types in the killifish testis, including selected marker genes. For germ cells, $ddx4^{high}$ marks Spermatogonia, and $ddx4^{low}$ marks Spermatocytes. Adapted from[1]. Center: smFISH for germ cells (*ddx4*, red) and Sertoli cells (*amh*, green). Right: smFISH for *vgll3* (green, top), and *vgll3* (red) and *amh* (green, bottom). Representative of $n \geq 6$ individuals. White asterisk marks autofluorescence from nucleated red blood cells. Scale bar: 10 μm.

Source data are provided as a Source Data file.

a. Nuptial coloration in 1-month-old fish

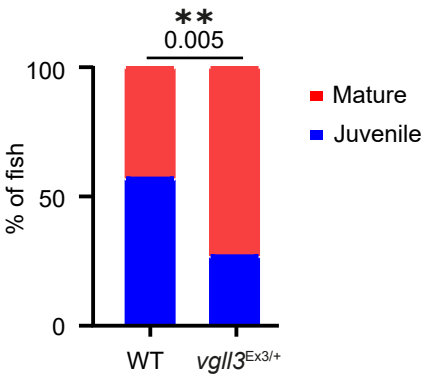

b. PCA for the transcriptome of primary fibroblasts

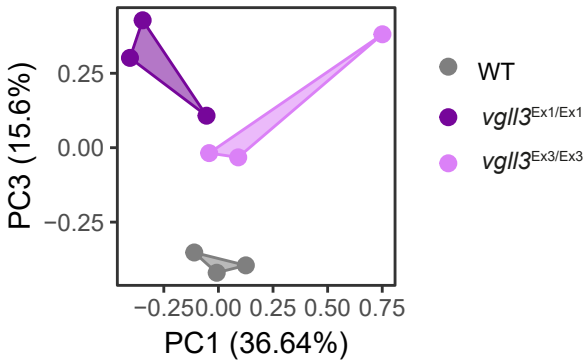

c. Laser-induced damage (LID)

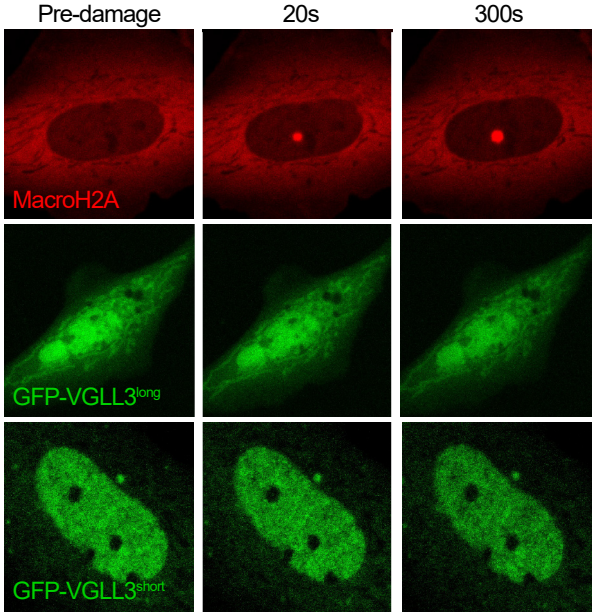

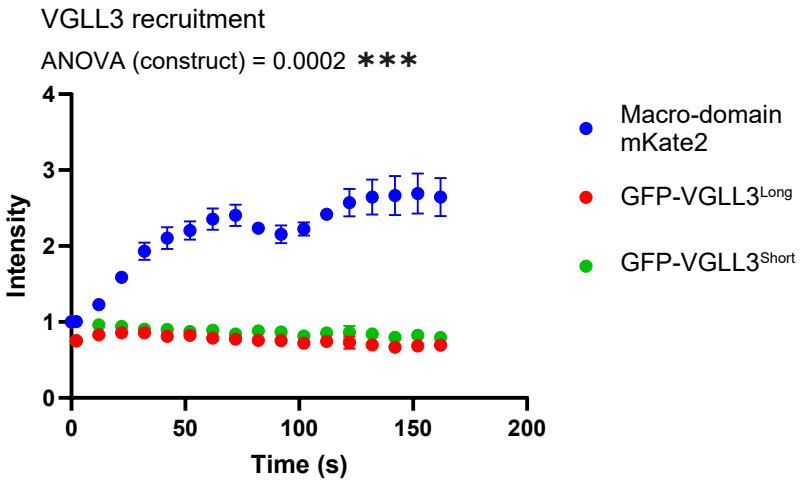

Supplementary Figure 2: Transcriptomic and phenotypic analysis of *vgll3* mutants

a) Proportion of fish displaying mature and juvenile coloration in 1-month-old WT (n = 14) and *vgll3*$^{Ex3/+}$ (n = 22) males. Significance was measured using a χ^2-test with the WT proportion as the expected value.

b) PC1/PC3 for transcript levels from primary fibroblast cultures. Each symbol represents an individual cell line (n = 3 independent cell lines for each genotype).

c) Left: Representative live-cell images showing recruitment of the macroH2A positive control (red) and GFP-tagged VGLL3 isoforms (green) following DNA damage induced by laser micro-irradiation ($n \geq 3$). Right: Quantification of fluorescence intensity at damage sites over time. Error bars: mean ± SEM; significance: repeated-measures ANOVA.

Source data are provided as a Source Data file.

a. Length of ~3 month old *vgll3*$^{Ex1/Ex1}$ males and females

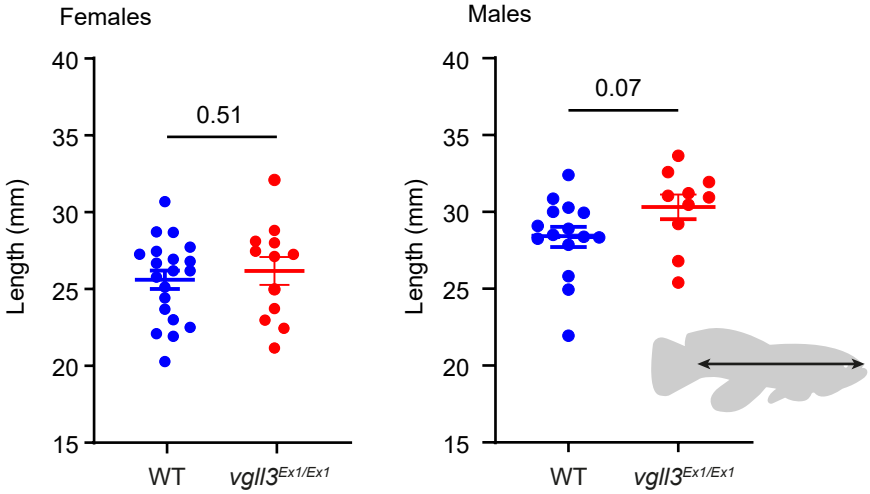

b. Depth of old *vgll3*$^{Ex1/Ex1}$ males

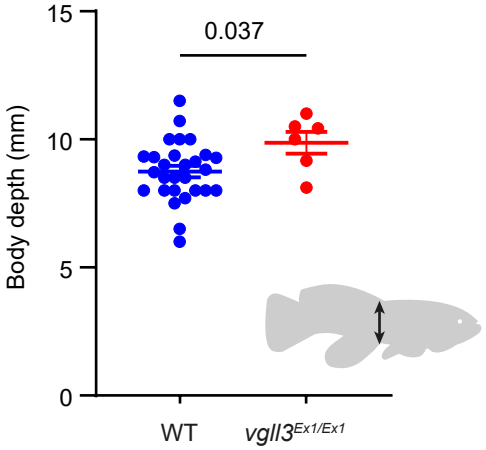

c. Testis weight and mature sperm content in 3 months old *vgll3*$^{Ex1/Ex1}$ mutants

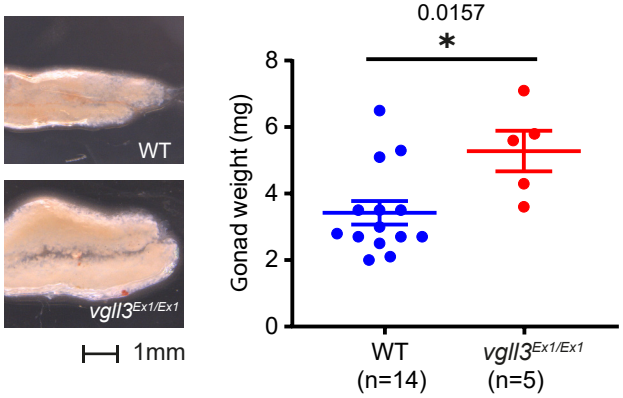

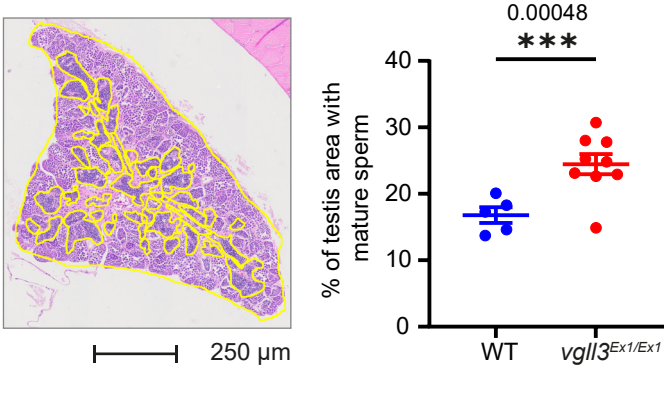

d. DNA damage in the testis of *vgll3*$^{Ex1/Ex1}$ mutants

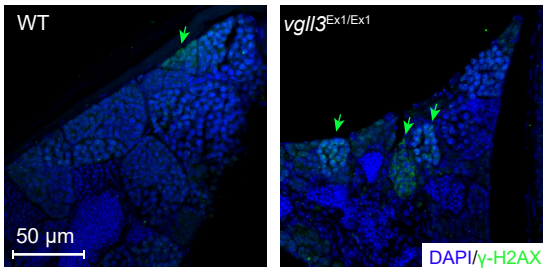

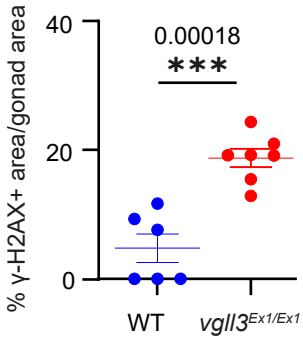

e. Age-related melanoma-like expansion in WT males

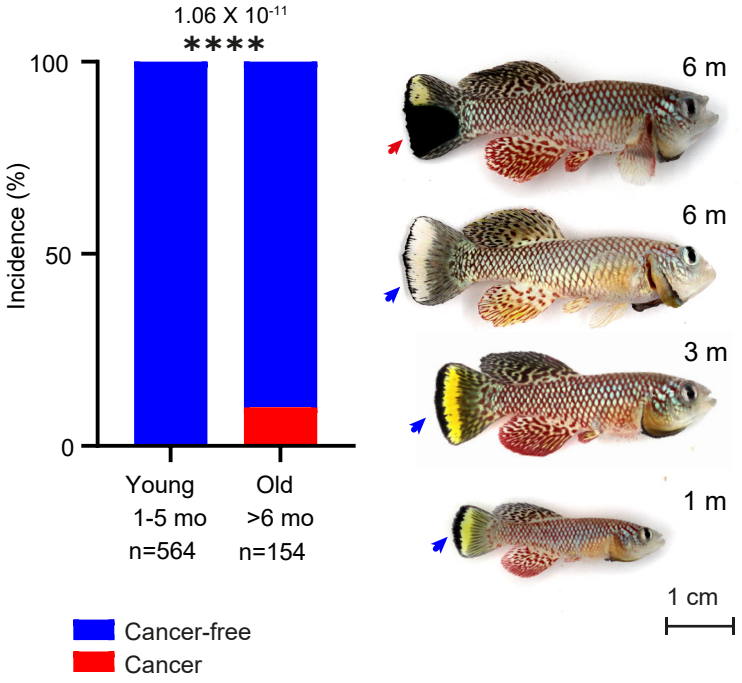

Supplementary Figure 3: Effects of *vgll3* exon 1 mutants on growth and sperm production

a) Quantification of length in three-month-old WT and *vgll3*$^{Ex1/Ex1}$ female (left) and male (right) fish. $n \geq 10$ fish per experimental group.

b) Quantification of depth (distance between dorsal and anal fins) in five-month-old WT and *vgll3*$^{Ex1/Ex1}$ male fish (n = 21, 6, respectively).

c) Left: representative images of gonads dissected from three-month-old WT and *vgll3*$^{Ex1/Ex1}$ male fish and quantification of gonad weight. Right: representative image of an H&E-stained testis (with Spermatozoa-containing cysts marked in yellow), and quantification of the relative area (%) containing spermatozoa from three-month-old fish. At least 5 histological sections from ≥ 3 fish. Scalebar: 250µm.

d) Top: Representative images of DNA damage in the testis of three-month-old WT and *vgll3*$^{Ex1/Ex1}$ mutant fish. Damage was immunoassayed by γ-H2AX staining (green) with DAPI (blue) for nuclei detection. Data collected from at least 2 images from n = 3 individuals. Scale bar: 50 µm. Bottom: quantification of the percentage of γ-H2AX positive area in the gonad.

e) Left: frequency of fish displaying large melanocyte expansions in < 6-month-old fish, and > 6-month-old WT individuals (n = 564, 154, respectively). Significance was calculated using Fisher's exact test. Right: representative images of old and young WT males. Melanocyte expansion is marked by a red arrow, and normal tails by blue arrows. Scale bar: 1 cm.

Unless mentioned otherwise, error bars: mean ± SEM. Significance: two-sided Student's t-test. Source data are provided as a Source Data file.

a. PCA for transcript levels in the head kidney

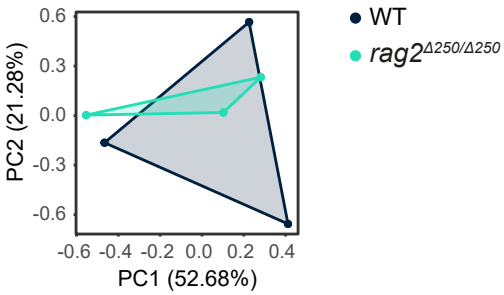

b. Barplot of selected up- and down-regulated genes

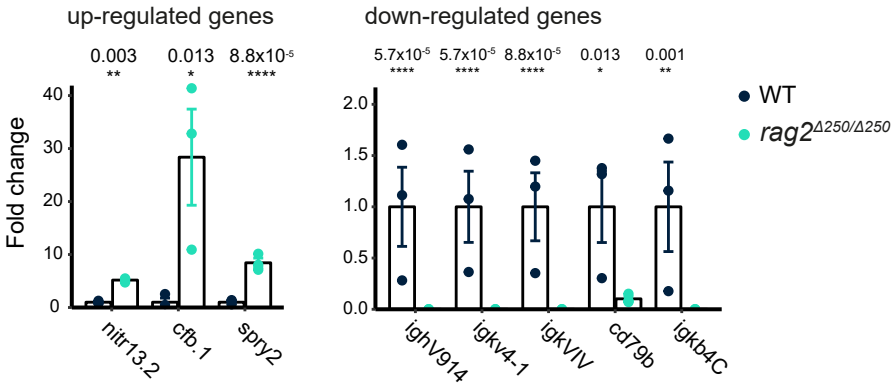

Supplementary Figure 4: Altered immunity in *rag2* mutant fish

a) PCA (PC1/PC2) for transcript levels shown in the **Figure 4a**, of WT (black) and *rag2*$^{\Delta 250/\Delta 250}$ mutant fish (green). Each symbol represents an individual fish. *n*=3 for each genotype.

b) Bar-plot of selected upregulated (left) and downregulated (right) genes, normalized to the WT. Error bars: mean ± SEM. Significance was called as part of the edgeR pipeline. FDR-corrected p-values are indicated.

Source data are provided as a Source Data file.

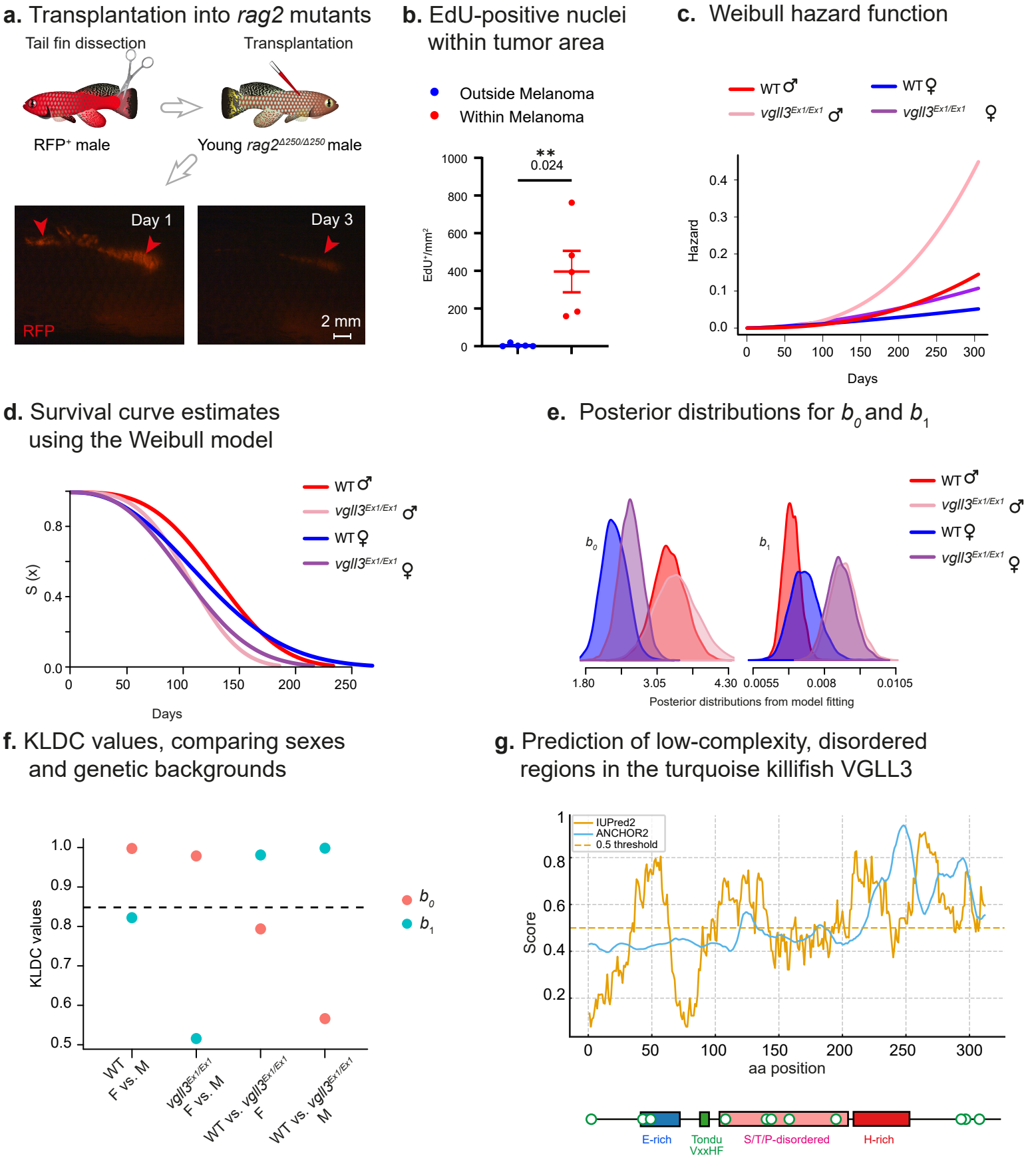
a. Transplantation into rag2 mutants
Tail fin dissection
Transplantation
RFP+ male
Young rag2Δ250/Δ250 male
Day 1
Day 3
RFP
2 mm
b. EdU-positive nuclei within tumor area
Outside Melanoma
Within Melanoma
**
0.024
EdU+/mm2
c. Weibull hazard function
WT ♂
vgll3Ex1/Ex1 ♂
WT ♀
vgll3Ex1/Ex1 ♀
Hazard
Days
d. Survival curve estimates using the Weibull model
S (x)
Days
e. Posterior distributions for b0 and b1
b0
b1
Posterior distributions from model fitting
f. KLDC values, comparing sexes and genetic backgrounds
KLDC values
WT F vs. M
vgll3Ex1/Ex1 F vs. M
WT vs. vgll3Ex1/Ex1 F
WT vs. vgll3Ex1/Ex1 M
g. Prediction of low-complexity, disordered regions in the turquoise killifish VGLL3
IUPred2
ANCHOR2
0.5 threshold
Score
aa position
E-rich
Tondu VxxHF
S/T/P-disordered
H-rich

Supplementary Figure 5: Transplantation assay and actuarial senescence

a) Injection of RFP^+-derived primary cells into WT fish ($n = 10$ biological replicates). Following injection of WT, non-malignant cells into *rag2* models, these cells are rapidly cleared, so that 3 days post-injection, RFP expression is hardly detected.

b) Quantification of the density of EdU^+ nuclei within and outside the area populated by tumor-like cells, n=5 images. Error bars: mean ± SEM. Significance: two-sided paired Student's t-test.

c) Hazard function changes with age from the fitted parametric Weibull regression analysis across treatments.

d) Survival curve estimates as fitted from the simple Weibull model.

e) The posterior distributions of b0 and b1 mortality parameters, which, according to the simple Weibull formula ($\mu_0(x|b) = b_0 b_1{}^{b0} x^{b0-1}$), describe either baseline mortality (*b0*) or mortality rate change with age (b1). The non-overlapping distributions for the *b1* mortality parameter between *vgll3* mutants and WTs indicate a substantial difference between these treatments. Using BaSTA with the best-fitting Weibull model (see **Methods**), we found no difference in baseline mortality between $vgll3^{Ex1/Ex1}$ mutants relative to WTs for either sex (although females had lower baseline mortality rates compared to males).

f) The posterior distributions of mortality parameters (in panel **e**) were compared between conditions using Kullback–Leibler divergence calibration (KLDC). KLDC values closer to 0.5 indicated minimal difference between the distributions, and values approaching 1 implied a larger difference[2,3]. We considered a KLDC value > 0.85 to indicate a substantial difference between treatments[4,5].

g) Top: IUPred2A[6] predictions of intrinsically disordered regions (IUPred2, orange) and disordered binding regions (ANCHOR2, blue). Bottom: Protein domain architecture (color-coded boxes) with amino-acid residues under positive selection marked by green circles (E5D, S40C, P47L, V108I, P136A, S140A, I154V, T194S, T285S, P294S, P310S). Trimmed protein sequences from Cui et al[7] are provided in **Table S1**). Residue numbers are shown on the x-axis; disorder scores range from 0 to 1 with a 0.5 threshold.

Source data are provided as a Source Data file.

References:

1. Moses, E., Atlan, T., Sun, X., Franěk, R., Siddiqui, A., Marinov, G.K., Shifman, S., Zucker, D.M., Oron-Gottesman, A., Greenleaf, W.J., et al. (2024). The killifish germline regulates longevity and somatic repair in a sex-specific manner. Nat. Aging, 791–813. 10.1038/s43587-024-00632-0.

2. McCulloch, R.E. (1989). Local Model Influence. J. Am. Stat. Assoc. *84*, 473–478. 10.2307/2289932.

3. Kullback, S., and Leibler, R.A. (1951). On information and sufficiency. Ann. Math. Stat. *22*, 79–86.

4. Rodríguez-Muñoz, R., Boonekamp, J.J., Fisher, D., Hopwood, P., and Tregenza, T. (2019). Slower senescence in a wild insect population in years with a more female-biased sex ratio. Proc. R. Soc. B *286*, 20190286.

5. Spagopoulou, F., Teplitsky, C., Chantepie, S., Lind, M.I., Gustafsson, L., and Maklakov, A.A. (2020). Silver-spoon upbringing improves early-life fitness but promotes reproductive ageing in a wild bird. Ecol. Lett. *23*, 994–1002.

6. Mészáros, B., Erdős, G., and Dosztányi, Z. (2018). IUPred2A: context-dependent prediction of protein disorder as a function of redox state and protein binding. Nucleic Acids Res. *46*, W329–W337.

7. Cui, R., Medeiros, T., Willemsen, D., Iasi, L.N.M., Collier, G.E., Graef, M., Reichard, M., and Valenzano, D.R. (2019). Relaxed Selection Limits Lifespan by Increasing Mutation Load. Cell *178*, 385-399 e20. 10.1016/j.cell.2019.06.004.